Exciton-Optical Properties of TlBr and TlCl†

ROBERT Z. BACHRACH* AND FREDERICK C. BROWN
Department of Physics and Materials Research Laboratory, University of Illinois, Urbana, Illinois 61801
(Received 14 August 1969)

The effect of strain on thallous-halide films has been investigated, and a technique developed for producing essentially strain-free films. The optical absorption of strain-reduced TlBr and TlCl films has been measured down to 4.2°K, and the results analyzed for the optical constants. Relatively narrow (2-meV) first-exciton lines were found in the near ultraviolet accompanied by longitudinal-optical-phonon sidebands. The Faraday rotation pattern was measured through the first peak in TlBr and found to be linear in H. An analysis of the rotation pattern together with the known n and κ yields an exciton effective g value of 0.7 for TlBr. Oscillatory magnetoabsorption has been observed in both TlBr and TlCl originating from the edge of the sideband. The exciton binding energies are 6.5±1 meV in TlBr and 11±2 meV in TlCl. The exciton-optical transition is discussed and the importance of lattice and polaron effects emphasized.

I. INTRODUCTION

THE characteristic optical spectrum of a solid obtained from the transmission of thin films is sometimes quite different than that obtained from the reflectivity of bulk crystals. In the case of thin evaporated films on a substrate, this is largely due to strain introduced during deposition or during cooling. In the present work, a degree of control has been achieved over strain in films of the thallous halides evaporated at room temperature and then cooled to liquid-helium temperature for measurement purposes. Exceptionally sharp intrinsic exciton structure has been revealed and the exciton Faraday rotation pattern of TlCl and TlBr observed. A combination of optical and magneto-optical experiments using a strain-reduced film (SRF) technique has yielded a knowledge of exciton parameters such as binding energy and effective g factor. It has also led to the discovery of an exciton-longitudinal optical-phonon sideband as well as the direct observation of oscillatory magnetoabsorption in these wide-band-gap ionic crystals.

A compilation of certain lattice and optical properties of TlBr and TlCl is shown in Table I. Both TlCl and TlBr are cubic and have the CsCl crystal structure. Among the interesting features of these materials are their large dielectric constant with its unusual temperature dependence (the static constant ϵ_s increases with decreasing temperature in the very low-temperature range), the rather unique, and in some ways simple, band structure in which both electrons and holes are mobile, the temperature dependence of the band gap, and the low-lattice frequencies with large anharmonic effects. Polaron effects are important in the thallous halides and they fall well within the intermediate coupling regime. Coupling between the electron and the lattice system will be further discussed in connection with excitons in Sec. V. Meanwhile we turn to experimental details including sample preparation.

II. SAMPLE PREPARATION

The SRF referred to above consists of a two-part substrate plus the evaporated thallous-halide film. The main part of the substrate is a single crystal (approximately 1×1×0.1 cm) of the material to be investigated (TlCl or TlBr) with a hole about $\frac{3}{16}$-in. cut in it. The hole is covered by a thin organic film onto which the thallous halide is evaporated. In most of the present work, a thin (approximately 250 Å thick) Lucite film was formed on water, picked up, and then placed over the crystal substrate. The technique for doing this is to place a lifter (an L-shaped piece of sheet metal with a hole in it slightly smaller than the crystal substrate) in a dish of water and then a drop of Lucite solution onto the water. After the organic film is formed, it can be removed from the water by slowly rotating and raising the lifter. The crystal substrate is then placed over the hole, and holding the crystal with a piece of filter paper, the assembly is turned over, and the substrate with film is removed.

A solution of Lucite is prepared by dissolving a weighed amount of Lucite plastic in ethylene dichloride and then diluting to the required concentration. The solution is completed by adding a trace amount of Formvar, typically 0.001 g/cc. A solution of 0.015 g/cc

TABLE I. Optical and lattice properties of the thallous halides with CsCl structure.

	TlCl	TlBr
Lattice constant	3.84 Å	3.97 Å
Density	7.004	7.453
Low temperature ϵ_s	37.6[a]	35.1[a]
Low temperature ϵ_0	5.1[b]	5.41[b]
$\hbar\omega_{LO}(k=0)$	174 cm^{-1} (21.5 meV)[a]	116 cm^{-1} (14.3 meV)[c]
Band gap at 4.7°K	3.41 eV	3.01 eV

[a] R. P. Lowndes, Phys. Letters **21**, 15 (1966).
[b] K. Hojendähl, Kgl. Danske Videnskab. Selskab, Mat.-Fys. Medd. **16**, No. 2 (1938).
[c] E. R. Cowley and A. Okazaki, Proc. Roy. Soc. (London) **A300**, 45 (1967).

† Work supported in part by the Advanced Research Projects Agency under Contract No. SD-131 and the U. S. Army Research Office under Contract No. ARO(D)-217.

* Work performed in partial fulfillment of the requirements for Ph.D. degree, University of Illinois. Present address: Bell Telephone Laboratories, Murray Hill, N. J.

yields a film approximately 270 Å thick with a 6-μliter drop size.

The SRF substrate (crystal with hole plus organic film) was placed in sample cartridges which were used throughout the evaporation and measurement. The cartridge technique facilitated handling and reduced breakage. An SRF assembly is durable, but nothing must come in contact with the organic film or the area close to the hole. Pressure gradients, large air currents, or too rapid cooling will break the substrate film. In evaporating onto an SRF substrate, heating must be minimized by using low-temperature sources and radiation shielding, and for higher melting point materials, slow evaporation rates.

The thallous-halide starting material for evaporation was Johnson-Matthey TlCl and Harshaw TlBr powder, both of which were dried under vacuum. The self-contained evaporator in each case was made from glass pipe including a 4-in. pipe joint for access. An external heater surrounded a small Vycor extension tube which served as a source. A vacuum of 10^{-6} Torr was achieved by means of a well-trapped oil-diffusion pump. The film thickness was measured during evaporation with a quartz crystal oscillator calibrated interferometrically. Relative thickness measurements were good to ± 2 Å and the absolute calibration was ± 20 Å. The thallous halides have high vapor pressures at elevated temperatures and deposition was performed well below the melting point. The evaporation rate used depended upon the thickness. For films greater than 500 Å thick, rates from 50–100 Å/min were used while for films on the order of 200 Å thick, rates from 3–10 Å/min were used. Faster evaporation for the thinner films generally seemed to lead to films with light leaks, perhaps due to the formation of islands.

The films were maintained in a dry-nitrogen atmosphere during transfer from the evaporator to the cryostat to prevent degradation of the surface. The films and materials were handled under red light at room temperatures. Effects attributable to photolysis were not observed.

III. STRAIN IN THALLOUS-HALIDE FILMS

The SRF film-fabrication technique was developed when problems identified with strain effects arose during optical-absorption measurements and Faraday rotation experiments. Initially films were made on fused quartz substrates and results essentially in agreement with those in the literature were found.[1] In carrying out the program discussed below to determine the optical constants, it became clear that all the observed structure was not intrinsic. In the next experiment a single-crystal alkali-halide substrate was tried. The previously poorly defined structure split into two well-resolved peaks and the peak position shifted. To clarify any possible differences in crystallization, reflection electron-diffraction pictures were also taken. These showed that the degree of crystallization on the fused quartz and alkali-halide substrates was essentially the same. The only differences found in these experiments ascribable to the various substrates used were due to changes in the strain condition of the film.

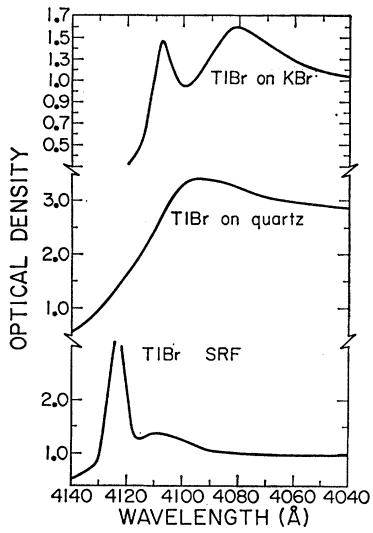

FIG. 1. Optical-density spectra of different thickness TlBr films on various substrates: (a) KBr, (b) quartz, (c) strain relieved film (the phonon sideband on the high-energy side of the peak is intrinsic and not associated with strain).

The SRF construction was developed to eliminate strain. Figure 1 indicates the kind of results obtained for films of TlBr evaporated onto KBr, quartz, and finally the SRF composite. Several features are readily apparent. The splitting of the first strong absorption band, the peak position, and the linewidth change with substrate (mainly due to variations in the strain condition rather than film thickness). Some small thickness dependence remained but, in the case of the TlBr SRF configuration, the residual splitting in the first peak was less than 0.5 meV. TlCl seemed to be even more susceptible to strain with large shifts and broadening evident. The SRF technique eliminated most of this except for splittings in the main peak of 3–6 meV. The experiments discussed below show that the structure such as shown in Fig. 1(a) is due to the removal of electronic degeneracy. In summary, as the strain increases, the first peak splits and broadens, and the absorption shifts to higher energies. If the strain is sufficiently large, intrinsic structural detail such as the phonon sideband[2] becomes completely masked.

A small amount of residual splitting remained for SRF films. The residual splitting and position of the first peak varied slightly from film to film. This effect was most pronounced in TlCl. The temperature de-

[1] S. Tutihasi, Phys. Chem. Solids **12**, 344 (1959); H. Zinngrebe, Z. Physik **154**, 495 (1959).

[2] R. Z. Bachrach and F. C. Brown, Phys. Rev. Letters **21**, 685 (1968); Bull. Am. Phys. Soc. **14**, 558 (1969).

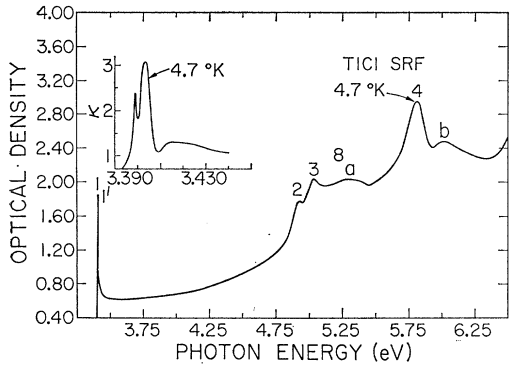

FIG. 2. The optical-density spectra of TlCl SRF. The extinction in the vicinity of the first line is also shown on an expanded scale.

pendence of the splitting suggested that differential thermal expansion and strain were causing the splitting. Several experiments showed directly that the splitting of the first exciton peak in TlBr and TlCl was associated with the removal of degeneracy of noncubic strains. One experiment involved applying a uniaxial stress to a film of TlBr evaporated onto a KBr crystal surface. Both stress-induced optical absorption and linear dichroism were investigated. Upon applying uniaxial stress the position of the maximum absorption could be changed, and the movement was reversible as long as the substrate was not plastically deformed. This result shows how tightly bound the films are to the substrate. A free single crystal of the thallous halides would not support as large a stress without plastically deforming. A linear dichroism signal was also observed indicating that, in fact, the uniaxial component of the stress will remove the electronic degeneracy. The other experiment was the measurement and correlation of intrinsic stress birefringence with features of the optical absorption. An experiment was also performed with a metal substrate in which large differential contractions occurred and the peak splitting was increased.

Strain (or stress) in thin films initially arises from the condensation of the evaporated material onto the substrate. The mechanism of the straining is not fully understood. However, it is primarily related to how the deposited material interacts with the substrate, and not to thermal-expansion differences.[3] The deposition stress is thickness-dependent and can become quite large.[4] The other origin of stress arises with changes due to differences in thermal expansion of the film and substrate. With a thick substrate, the strain that develops is essentially determined by the substrate, and the stress birefringence pattern cannot be analyzed on the basis of a simple model. On the other hand, the stress distribution in an SRF film is essentially uniaxial. Moreover the thicker evaporated films exhibited less strain, indicating some stress relief due to deformation of the thin substrate.

[3] M. Francombe and H. Sato, *Single Crystal Films* (Pergamon Press, Inc., New York, 1964).
[4] A. Ennos, Appl. Opt. 5, 51 (1966).

IV. OPTICAL ABSORPTION OF THIN FILMS

The optical absorption of the thin-film samples was measured with a Cary 14R spectrophotometer with the films mounted in a variable temperature cryostat using proportional temperature control. Low temperatures were measured with a germanium thermometer and high temperatures with a copper-constantan thermocouple referenced to ice water. The optical-absorption data was analyzed using a two-thickness subtraction method to yield the extinction coefficient, and then a subtracted dispersion relation was used to obtain the index of refraction. In the two-thickness method, the extinction coefficient is given by

$$\kappa = 2.303 \frac{\lambda}{4\pi} \frac{[(D_1 - D_2) + \log_{10}(f_2/f_1)]}{d_1 - d_2}, \qquad (1)$$

where the D's are the optical densities. The correction term $c = \log_{10}(f_2/f_1)$ incorporates reflectivity and surface effects. This term was investigated for various values of n, κ, and thickness, and found to be small for the thallous halides in the spectral region of interest. The extinction coefficient could therefore be obtained to about 10% accuracy by setting $\log_{10}(f_2/f_1) = 0$ in Eq. (1). Problems arose in applying the method because of stress changes from film to film and because it was not possible to accurately present the first exciton peak, the sideband, and the absorption at higher energy with only two films. Recourse was taken to using several films chosen with comparable stress levels. The extinction coefficient values found were compared and agreement obtained for various film thicknesses. Care was taken to determine that the thinner films did not have light leaks.

Once the extinction coefficient has been obtained, the index of refraction can be calculated from a Kramers-Kronig relation usually of the form

$$n(\omega_p) - 1 = \frac{2}{\pi} \mathbf{P} \int_0^\infty \frac{\omega \kappa(\omega) d\omega}{\omega^2 - \omega_p^2}. \qquad (2)$$

The main drawback of this dispersion formula is that κ should be known for all ω, since the integral converges slowly as $\omega \to \infty$. If the index of refraction is known at some frequency ω_0, for example, in the transparent region from a refractometer measurement, the accuracy of the index obtained can be improved by using a subtracted dispersion relation as follows:

$$n(\omega_p) = n(\omega_0) + \frac{2}{\pi} (\omega_p^2 - \omega_0^2) \mathbf{P} \int_0^\infty \frac{\omega \kappa(\omega) d\omega}{(\omega^2 - \omega_0^2)(\omega^2 - \omega_p^2)}. \qquad (3)$$

The subtracted form of the dispersion relation has the advantage that the integral converges rapidly and one

TABLE II. Peak positions in the thallous halides —4.7°K. The identifying numbers refer to the structure labeled in Figs. 2 and 3. Spin-orbit splitting on the thallium is indicated by the separation 4–1; on the halogen by 3–2.

	TlCl SRF			TlBr SRF	
	λ (Å)	E (eV)		λ (Å)	E (eV)
1	3644	3.402	1	4122	3.007
1′	3624	3.422	1′	4104	3.021
2	2518	4.924	2	3064	4.046
3	2468	5.024	3	2774	4.469
4	2133	5.813	4	2460	5.040
5			5	2034	6.10
a	2338	5.30	*a*	2366	5.24
b	2068	6.00	*b*	2138	5.8
4–1	(Tl^+)	2.41	4–1	(Tl^+)	2.03
3–2	(Cl^-)	0.10	3–2	(Br^-)	0.43

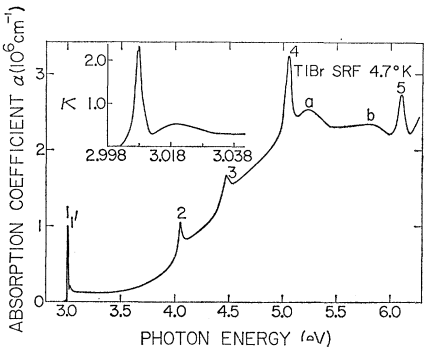

FIG. 3. The optical-density spectra of TlBr SRF. The extinction in the vicinity of the first line is also shown on an expanded scale.

can obtain accurate results for a restricted wavelength region without measuring κ over all energies. In fact, to obtain the index of refraction in the restricted range, κ need only be known over a moderately larger range. The integral result is fairly insensitive to the method of cutoff.

Figure 2 shows the optical-density spectra of TlCl SRF and Fig. 3 TlBr SRF. The peak positions at 4.7°K are summarized in Table II. The band structure responsible for the spectra has been discussed previously.[2] It can be argued that the transitions are direct transitions and that they involve initial and final states on the thallous ion at least at the threshold. Using atomic notation, peak 1 corresponds to an excited $^3P_1$ configuration (with admixture of singlet due to spin-orbit coupling) whereas peak 4 corresponds to $^1P_1$. Peaks 2 and 3 involve the halide sublattice. Preliminary band calculations (Kunz) indicate that the transitions on Tl^+ are at the point R and the transitions on the halide ions at Γ in the Brillouin zone. The primary concern of this paper is the first exciton peak and its associated phonon sideband labeled (1) and (1′), respectively, in Fig. 2. The first peak and phonon sideband can also be seen clearly in the case of TlBr (see Fig. 3 insert).

Figure 4 shows the temperature dependence of the first peak in TlBr and Fig. 5 shows the sideband as a function of temperature in a somewhat thicker sample. Similar results are obtained for TlCl. In both TlBr and TlCl, the peak shifts monotonically to lower energy with decreasing temperature, and the peak narrows. Although the exciton peak position shifts in energy with temperature, the peak-to-sideband spacing remains constant. The sideband shape is rather insensitive to temperature as seen in Fig. 5. At high temperatures the main peak broadens sufficiently to cover the sideband.

The Debye temperature for TlBr is lower than for TlCl, so that the peak broadens appreciably at much lower temperatures. In thicker films of TlBr, where the sideband was well resolved or, correspondingly, the strain low, the main peak appeared to continue to narrow to helium temperature. Attempts to observe this in films thin enough to determine a linewidth were

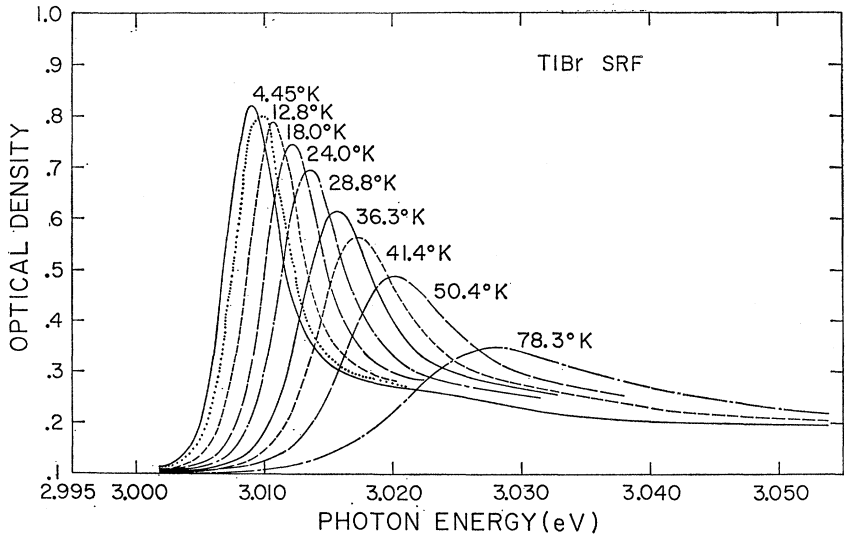

FIG. 4. The temperature dependence of the first exciton peak in TlBr SRF.

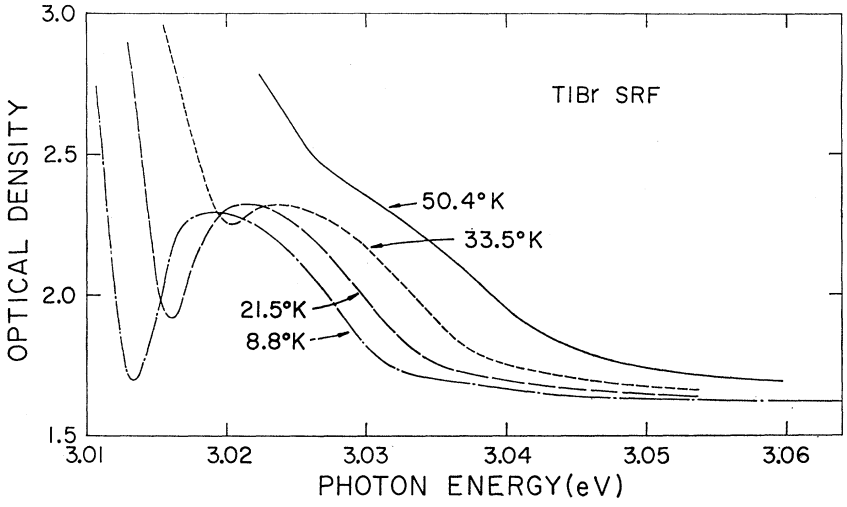

FIG. 5. The temperature dependence of the sideband in TlBr SRF. A somewhat thicker film was used than in Fig. 4.

unsuccessful because residual stresses still dominated. The linewidths obtained at low temperatures in the current experiment are clearly still not the intrinsic linewidths in the absence of strain. In all likelihood, the intrinsic unstrained linewidth is at least a factor of 2 less than that observed.

The optical-absorption data were analyzed using the two-thickness subtraction method and then the subtracted dispersion relation applied to obtain the index of refraction. These are plotted in Fig. 6 for TlBr. Figure 7 shows the single-crystal reflectivity spectra expected in TlBr calculated from the index of refraction and extinction coefficients obtained in the present work. One of the surprising features is the double reflectivity peak associated with the single absorption peak. The small peak occurs when n is a maximum and κ is small; the large peak occurs when κ is a maximum and n is small. A double peak such as this would not occur for a simple oscillator. Apparently the exciton resonance in these materials is more complicated. Errors in the line shapes obtained for n and κ might also cause a double peak, but we think that this is not the case here. Structure has been reported in the measured reflectivity of TlBr.[5]

As is well known, the imaginary part of the dielectric response function $\epsilon_2 = 2n\kappa$ relates most closely to the effect of an electromagnetic field on an electronic system. It is the product of n and κ which is most directly related to transition rates. Figure 8 shows both the real and the imaginary parts of the dielectric response function for TlBr. Several features have appeared in ϵ_2 that were not apparent in the original optical data or in κ alone. The peak in ϵ_2 is somewhat sharper than in κ, and also it is shifted about 1 meV to lower energy. The small peak separated by about 4.5 meV is felt to represent higher exciton states $n=2\rightarrow\infty$. Corresponding structure appears in the Faraday rotation experiment. Assuming a hydrogenic series, this structure yields a binding energy for the exciton in TlBr of 6 ± 1 meV. The sideband is found to be separated from the main peak by roughly $\hbar\omega_{LO}$ in ϵ_2 as compared with $0.82\,\hbar\omega_{LO}$, estimated directly from the optical absorption.[2] The oscillator strength of the first exciton line as estimated from its area is 3×10^{-3}. Oscillator strength ratios of $\frac{1}{8}$ for the $n=2\rightarrow\infty$ peak and $\frac{1}{3}$ for the sideband were obtained. Two other features of ϵ_1 and ϵ_2 are worth observing. One is that the first zero in ϵ_1 occurs at the peak energy of ϵ_2 as one would expect (unlike n and κ). The other feature is that the zero to higher energy corresponds to the longitudinal exciton which is optically inactive. The longitudinal transverse-exciton splitting in TlBr is probably of the order of 2 meV.

The optical constants of TlCl were obtained in the same manner as for TlBr. More problems were encountered, however, because of the large residual stress splitting. The criteria used in selecting the TlCl films for the analysis was that the structure separation in the main peak was about the same and that the sidebands had comparable resolution. One surprising feature was

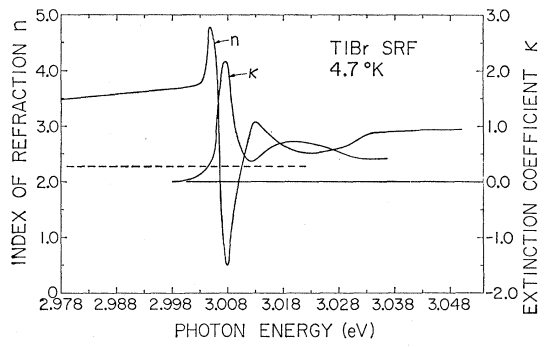

FIG. 6. The optical constant spectra of TlBr in the vicinity of the first exciton peak.

[5] A. Feldman, Bull. Am. Phys. Soc. 14, 428 (1969).

that, whereas the absorption data indicated that the first peak splits into unequal width peaks, ϵ_2 indicates that the two main peaks are of comparable width and strength. A small additional peak appears in ϵ_2 for TlCl as was the case for TlBr. Allowing for strain splitting, two separate exciton series are formed and the binding energy in TlCl is 10 ± 1 meV (estimated from the $n=1$, 2 separation). Since actually the strain splitting is comparable to the exciton binding energy, it is difficult to accurately determine the exciton binding in this case. The difficulty of assigning an energy separation to the phonon sideband is accentuated in TlCl: The first peak which has residual splitting is accompanied by a broad flat sideband with only a hint of structure in it. As in TlBr, however, the centroid spacing of the sideband from the centroid of the split main peak is more nearly $\hbar\omega_{LO}$ than had been estimated from the raw absorption data. The sideband threshold in both cases is considerably reduced in energy from $\hbar\omega_{LO}$. One would expect the sideband peak to occur at an energy greater than $\hbar\omega_{LO}$.

The oscillator strength for the first exciton peak in TlCl is 5×10^{-3} and the peak-to-sideband oscillator-strength ratio is about $\frac{1}{4}$. A comparable oscillator strength was found for TlCl on quartz data, showing that, within experimental error, the oscillator strength remains constant under stress perturbation.

V. FARADAY ROTATION AND MAGNETOABSORPTION

Both Faraday rotation and magnetoabsorption experiments were carried out in the vicinity of the first exciton line, and the results show that the magnetic perturbation is a valuable tool for probing the exciton structure. The magnetic experiments were only possible because of the strain reduction achieved using the techniques described in Sec. II.

A. Experimental

The magneto-optical experiments were carried out with an apparatus equipped for measuring optical absorption using either linear or circular polarized light (see Fig. 9). A 200-W quartz-iodine lamp and a Leiss monochromator modified with a 1200-line/mm grating served as a light source. A measured resolution of better than $\frac{1}{2}$ Å was available. The light from the monochromator was deflected upwards by means of a front-silvered mirror and focused with a quartz lens onto the sample located in the middle of a 50-kG superconducting solenoid. The first polarizer was mounted just above the monochromator in a calibrated rotatable holder. A recess was provided into which a quarter-wave plate could be inserted and accurately positioned with respect to the polaroid angular position. The polaroids used were either Polacoat type PL40 on Suprasil or Polaroid type HNP-B.

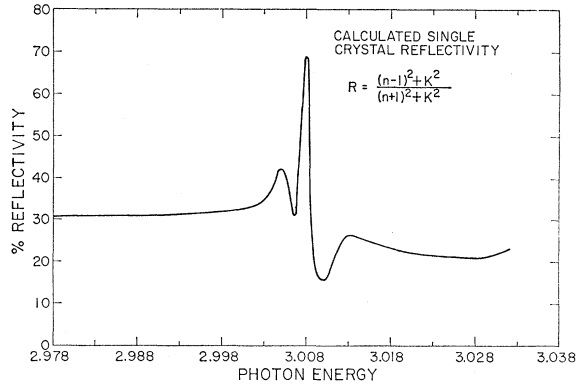

FIG. 7. The calculated reflectivity spectra for TlBr SRF.

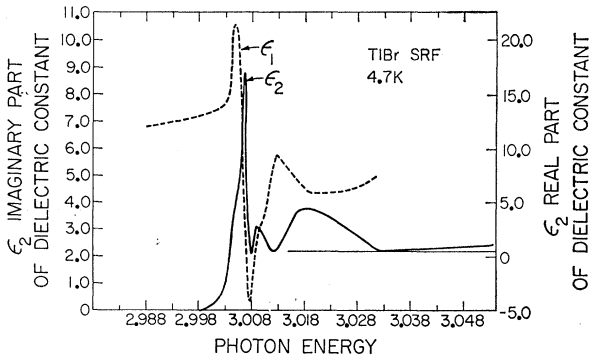

FIG. 8. The response function spectra for TlBr SRF.

Light transmitted by the sample was collected with an electropolished stainless-steel light pipe and detected with a photomultiplier (RCA type 1265 or EMI type 9558Q). The light pipe was very efficient and did not measurably affect the polarization. For the Faraday rotation measurement, ac sample and reference signals were generated by a rotating polaroid situated just before the photomultipliers. The output of the sample channel was kept constant to within a few tenths of a volt by an analog feedback drive applied to the photomultiplier power supply. The output signals were amplified with a matched pair (within $\frac{1}{2}$% gain, Q, and frequency) of tuned linear amplifiers and then further amplified to drive an Ad-Yu model-405 phasemeter which drove a strip-chart recorder through a scale-shifting circuit. The scale shifter permitted a scale expansion by ±5 full scale widths. The smallest detectable phase angle was less than 0.03° at an optical-density of 2. Optical absorption was measured by removing the photomultiplier control and detecting the output with a lock-in amplifier. The Faraday rotation pattern could therefore be compared with the optical-density spectra obtained either in the same apparatus or separately by means of a Cary model-14R spectrophotometer.

B. Faraday Rotation in Strongly Absorbing Cubic Media

In the Faraday geometry a plane polarized light wave propagates parallel to the direction of an applied

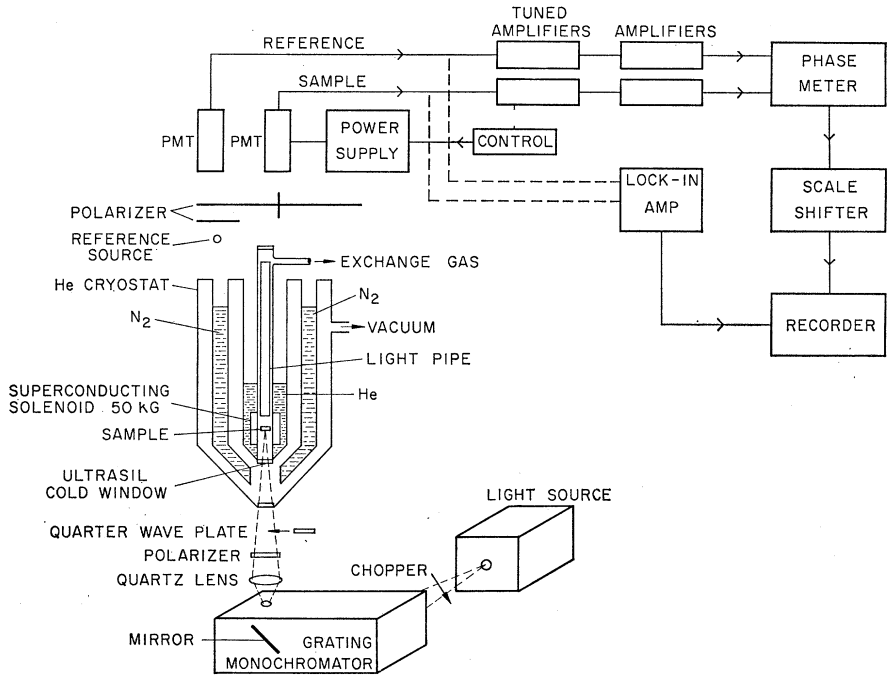

FIG. 9. The Faraday rotation and magnetoabsorption apparatus.

magnetic field **H**. Let us assume **H** and the propagation vector **k** lie in the positive z direction. A positive Faraday rotation therefore corresponds to a counterclockwise rotation of the electric field vector in the x-y plane as viewed by an observer looking opposite to the direction of propagation. A linearly polarized wave can be decomposed into right and left circularly polarized components $E(\mathbf{r},t)=E_r(\mathbf{r},t)+E_l(\mathbf{r},t)$ as follows:

$$\mathbf{E}_r(\mathbf{r},t)=E_0(\hat{x}-i\hat{y})e^{i(k_rz-\omega t)}, \tag{4a}$$

$$\mathbf{E}_l(\mathbf{r},t)=E_0(\hat{x}+i\hat{y})e^{i(k_lz-\omega t)}. \tag{4b}$$

We use the conventional definition of right-circular polarization, i.e., the electric vector E_r at a fixed point on the z axis rotates clockwise as viewed by an observer looking opposite to the direction of rotation (for an atomic system E_r would induce transitions $\Delta m=-1$). The $e^{-i\omega t}$ time dependence of Eqs. (4) implies a complex dielectric response function

$$\tilde{\epsilon}=\epsilon_1+i\epsilon_2 \tag{5}$$

and a similar relation for the complex index $\tilde{n}=n+i\kappa$. This is the convention used by some authors[6,7] but it is the complex conjugate of that employed by others.[8,9]

When a magnetic field is present, the dielectric response function is a tensor with complex components as follows[9]:

$$\tilde{\epsilon}=\begin{bmatrix}\epsilon_{xx} & \epsilon_{xy} & 0\\ -\epsilon_{xy} & \epsilon_{xx} & 0\\ 0 & 0 & \epsilon_{zz}\end{bmatrix}. \tag{6}$$

It is not difficult to show that this is the correct form for $\tilde{\epsilon}$ when **H** is oriented along the $\langle 100\rangle$ axes of a cubic crystal.[10] The same form applies for arbitrary orientation provided one is only interested in effects which are linear in **H**.

Now for convenience let us define a dielectric function and a complex index appropriate to right and left circularly polarized waves:

$$\tilde{\epsilon}_{r,l}=\tilde{\epsilon}_{xx}\mp i\tilde{\epsilon}_{xy} \tag{7}$$

and

$$\tilde{n}_{r,l}=n_{r,l}+i\kappa_{r,l}=(c/\omega)\tilde{k}_{r,l}. \tag{8}$$

By using these definitions and inserting Eqs. (4) into Maxwell's equations it can be shown that

$$\tilde{\epsilon}_{xx}-i\tilde{\epsilon}_{xy}=\tilde{\epsilon}_r=\tilde{n}_r^2=(c^2/\omega^2)\tilde{k}_r^2, \tag{9a}$$

$$\tilde{\epsilon}_{xx}+i\tilde{\epsilon}_{xy}=\tilde{\epsilon}_l=\tilde{n}_l^2=(c^2/\omega^2)\tilde{k}_l^2, \tag{9b}$$

$$n_{r,l}^2-\kappa_{r,l}^2=\epsilon_{xx}^{(1)}\pm\epsilon_{xy}^{(2)}, \tag{10a}$$

$$2n_{r,l}\kappa_{r,l}=\epsilon_{xx}^{(2)}\mp\epsilon_{xy}^{(1)}, \tag{10b}$$

$$n_l\kappa_l-n_r\kappa_r=\epsilon_{xy}^{(1)}=\epsilon_l^{(2)}-\epsilon_r^{(2)}, \tag{11a}$$

$$(n_r^2-n_l^2)-(\kappa_r^2-\kappa_l^2)=2\epsilon_{xy}^{(2)}=\epsilon_l^{(1)}-\epsilon_r^{(1)}. \tag{11b}$$

[6] F. Stern, in *Solid State Physics*, edited by F. Seitz and D. Turnbull (Academic Press Inc., New York, 1963), Vol. 15.
[7] M. Born and E. Wolf, *Principles of Optics* (Pergamon Press, Inc., New York, 1965).
[8] F. C. Brown and G. Laramore, Appl. Opt. **6**, 669 (1967); see also F. C. Brown, B. C. Cavenett, and W. Hayes, Proc. Roy. Soc. (London) **300**, 78 (1967).
[9] I. M. Boswarva, R. H. Howard, and A. B. Lidiard, Proc. Roy. Soc. (London) **269**, 125 (1962).
[10] H. S. Bennett, thesis, University of Maryland, 1960 (unpublished).

In these relations the superscripts (1) and (2) indicate real and imaginary parts, respectively.

Smith[11] has given a rigorous derivation of the dispersion relations connecting the various quantities in the above equations. The first of these are well known[9]:

$$\epsilon_{ij}^{(1)}-\delta_{ij}=\frac{2}{\pi}\mathbf{P}\int_0^\infty \frac{\omega_0}{\omega^2-\omega_0^2}\epsilon_{ij}^{(2)}(\omega)d\omega, \quad (12a)$$

$$\epsilon_{ij}^{(2)}=-\frac{2}{\pi}\mathbf{P}\int_0^\infty \frac{\omega_0}{\omega^2-\omega_0^2}\epsilon_{ij}^{(1)}(\omega)d\omega. \quad (12b)$$

The dispersion relations between n and κ in a magnetic field are not so well known and are given below:

$$\tfrac{1}{2}(n_r+n_l)-1=\frac{2}{\pi}\mathbf{P}\int_0^\infty \frac{\omega}{\omega^2-\omega_0^2}\tfrac{1}{2}[\kappa_r(\omega)+\kappa_l(\omega)]d\omega, \quad (13a)$$

$$n_r-n_l=\frac{2}{\pi}\mathbf{P}\int_0^\infty \frac{\omega_0}{\omega^2-\omega_0^2}(\kappa_r-\kappa_l)d\omega, \quad (13b)$$

$$\tfrac{1}{2}(\kappa_r+\kappa_l)=-\frac{2}{\pi}\mathbf{P}\int_0^\infty \frac{\omega_0}{\omega^2-\omega_0^2}\tfrac{1}{2}(n_r+n_l)d\omega, \quad (14a)$$

$$\kappa_r-\kappa_l=-\frac{2}{\pi}\mathbf{P}\int_0^\infty \frac{\omega}{\omega^2-\omega_0^2}[n_r-n_l]d\omega. \quad (14b)$$

The quantities on the left in Eqs. (13b) and (14b) are just what are measured in Faraday rotation and circular dichroism experiments, respectively. The Faraday rotation, the rotation of the plane of polarization, is given by

$$\theta_F=(n_r-n_l)(\pi d/\lambda) \quad \text{or} \quad \Delta n=(\lambda/\pi d)\theta_F, \quad (15a)$$

whereas the circular dichroism is given by

$$CD=(\kappa_r-\kappa_l)(4\pi d/\lambda) \quad \text{or} \quad \Delta\kappa=(\lambda/4\pi d)CD. \quad (15b)$$

The relations (13a) and (14a) can be seen to go over to the usual dispersion relations for n and κ at zero magnetic field.[6] In fact, to order linear in magnetic field, the relations

$$n=\tfrac{1}{2}(n_r+n_l), \quad (16a)$$

$$\kappa=\tfrac{1}{2}(\kappa_r+\kappa_l) \quad (16b)$$

are valid. This can be seen by inspection of Eq. (6) and noting how the components of $\tilde{\epsilon}$ enter into the polarization produced by a circularly polarized electric field. If the direction of propagation in the field is reversed, or alternatively $H\rightarrow -H$, left- and right-circular polarization interchange. This can only happen if, to order H, ϵ_{xx} is independent of magnetic field and ϵ_{xy} simply reverses sign with reversal of H. If one then reformulates the problem in terms of n_r and κ_r, it turns out that Eqs. (16a) and (16b) hold to first order in H.

[11] D. Y. Smith, International Symposium on Color Centers, Rome, 1968 (unpublished).

The Δn, $\Delta\kappa$, n and κ are all experimentally determined quantities. By combining $\Delta n=n_r-n_l$ and $\Delta\kappa=\kappa_r-\kappa_l$ with Eqs. (16), one obtains the following:

$$n_{r,l}=n\pm\tfrac{1}{2}\Delta n, \quad (17a)$$

$$\kappa_{r,l}=\kappa\pm\tfrac{1}{2}\Delta\kappa, \quad (17b)$$

$$\epsilon_{2r,l}=2n_{r,l}\kappa_{r,l}=2n\kappa\pm(n\Delta\kappa+\kappa\Delta n)+\tfrac{1}{2}\Delta n\Delta\kappa. \quad (18)$$

Generally speaking, the quantities of theoretical interest are the line-shape function $f(\omega)$ [12] and the changes in shape function Δf produced by the applied field. In the present work, it is convenient to define the line shape as equal to the imaginary part of the dielectric response $f=\epsilon_2$. The change in shape function upon application of H is therefore given by

$$\Delta f=\epsilon_{2r}-\epsilon_{2l}=2(n\Delta\kappa+\kappa\Delta n). \quad (19)$$

In the limit of weak absorption, Eq. (19) reduces to

$$\Delta f=\epsilon_{2r}-\epsilon_{2l}\cong 2n\Delta\kappa, \quad (20)$$

which is the form appropriate for absorption due to a dilute solution of defects such as F centers.[8] The limiting forms for the differences in n and κ are

$$n_r-n_l\cong\epsilon_{xy}^{(2)}/n, \quad (21)$$

$$\kappa_r-\kappa_l\cong\epsilon_{xy}^{(1)}/n. \quad (22)$$

Weak absorption due to a dilute impurity or defects requires that n is essentially constant and equal to the host index n_0 in the absorption region. At least in these limiting cases one sees that Faraday rotation or circular dichroism measurements are more directly related to certain individual components of the dielectric tensor $\tilde{\epsilon}$ than are optical-absorption measurements. One should not be surprised then to find the centers of Faraday rotation or circular dichroism patterns slightly shifted from the peak observed in optical absorption. We return to a discussion of the rotation patterns for the strong characteristic absorption in Sec. VI.

C. Faraday Rotation Results

Because of the residual splitting in TlCl, the most detailed Faraday rotation measurement was carried out on TlBr. No structure was contributed to the Faraday pattern by the substrate, and the constant background due to the fused-quartz windows plus the substrate was nulled out. Figure 10 shows a direct data scan in an exceptionally unstrained film. The Faraday pattern was found to scale linearly with field at least up to 50 kG. Notice that little or no rotation occurs in the region ($\sim$3.020 eV) of the phonon sideband. In thick films it was possible to detect a sideband rotation but it was barely above noise.

The main difficulty in the Faraday rotation experiment was the zero-field background associated with a small stress birefringence of the sample and substrate.

[12] M. Lax, J. Chem. Phys. **20**, 1752 (1952).

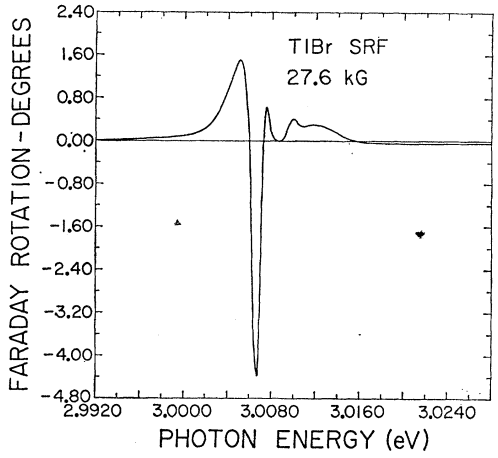

FIG. 10. The Faraday rotation spectra of TlBr SRF at 27.6 kG.

In all cases, the stress-birefringence pattern went quickly to zero in the wings outside the exciton peak. The procedure followed in obtaining the Faraday rotation was to set the first polaroid such that the zero-field pattern was a minimum. In addition, the Faraday rotation was measured with + and − fields and then $\theta'=\frac{1}{2}[\theta(+)-\theta(-)]$ taken as the real value. Such a procedure is valid as long as the Faraday rotation is linear in H.

The main features of Fig. 10 were reproducible from film to film. If the film is more strained, however, the pattern is broader, the peak rotations less, and the structure on the high-energy side of the pattern, although observable, becomes buried in the wing of the main peak. Since the structure is not related to the strain effect and lies between the main peak and the sideband, it is reasonable to attribute it to additional states. One sees that the minimum in Fig. 10 near 3.009 eV correlates well with the structure found in ϵ_2 which was likewise attributed to $n=2$ states of the exciton.

The film used in Fig. 10 was sufficiently unstrained that the zero-field effect was inconsequential. The structure in Fig. 13 was observable in fields as low as 1.5 kG. From the lowest to the highest fields, no change was observed in the position of the pattern minimum or in the separation of the structure to higher energies.

In order to analyze the observed rotation, the circular dichroism was taken as zero at zero energy and the dispersion relation for $\Delta\kappa$ [Eq. (14b)] was modified in the subtracted form

$$\kappa_r-\kappa_l=\Delta\kappa(E_p)=-\frac{4}{\pi}\frac{\hbar c}{d}E_p^2\mathbf{P}\int_0^\infty\frac{\theta(E)dE}{(E^2-E_p^2)E^2}. \quad (23)$$

The integral was then evaluated for the observed $\theta(E)$ with the use of a digital computer. For comparison, Fig. 11 shows $(n,\Delta n)$ and $(\kappa,\Delta\kappa)$ as a function of energy.

Since a direct Zeeman splitting cannot be resolved, one has to resort to a moments analysis to obtain an effective g value from Δn and $\Delta\kappa$. In the absence of an applied field the zeroth, first, and nth moments of the line shape $f\equiv\epsilon_2$ are defined by[13]

$$m^0=A=\int\epsilon_2(E)dE,$$

$$m^1=\bar{E}=\frac{1}{m^0}\int E\epsilon_2(E)dE, \quad (24)$$

$$m^n=\frac{1}{m^0}\int(E-\bar{E})^n\epsilon_2(E)dE, \quad n\geq 2.$$

We are especially interested in the changes in these moments due to the field. These changes can be computed from Δf as given by Eq. (19). The change in the zeroth moment, which is related to a change in oscillator strength of a band due to mixing should be quadratic in the field.

The change in the first moment

$$\Delta E=\frac{1}{A}\int(E-\bar{E})\Delta f dE \quad (25)$$

is linear in H and related directly to the exciton effective g value. Unfortunately, ΔE depends upon an accurate value for the first moment $\bar{E}$, and this is difficult to obtain with high precision from the ϵ_2 data. Only upper and lower estimates were obtained.

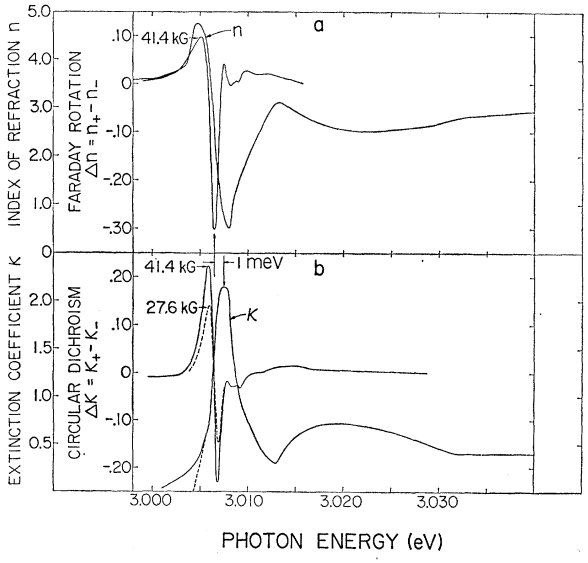

FIG. 11. The Faraday rotation and circular dichroism spectra of TlBr plotted with n and κ.

[13] C. H. Henry, S. E. Schnatterly, and C. P. Slichter, Phys. Rev. 137, 583 (1965).

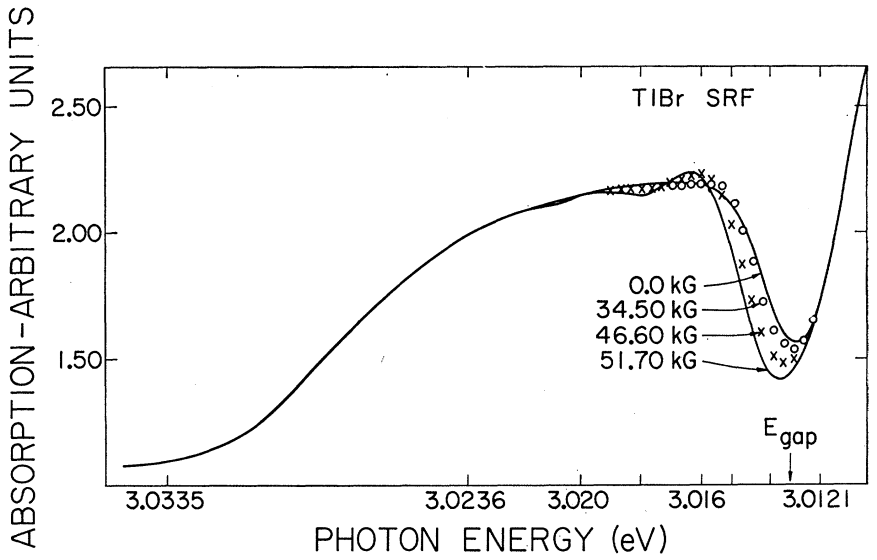

FIG. 12. The magnetoabsorption spectra of TlBr SRF at various magnetic fields.

An alternative analysis is to assume that the bands shift rigidly in the magnetic field. The Zeeman energy ΔE can then be determined directly. In the rigid-shift approximation the minimum Faraday angle

$$n_+ - n_-|_{E=E_0} = \Delta n|_{E=E_0} = (\partial n/\partial E)|_{E=E_0}\Delta E. \quad (26)$$

The derivative can be computed from the index of refraction curve (Fig. 11). Using this last equation a g value of 0.71 was obtained which lies between the upper and lower estimates from the moments analysis. Another procedure for determining the Zeeman splitting is to measure it from the curves $\epsilon_{2r,l}$ obtained by further decomposition.[14] Within experimental error, the peak separation for right and left polarization agreed with the rigid-shift approximation, i.e., 0.15±0.05 meV at 41.4 kG.

D. Magnetoabsorption

The effect of a longitudinal magnetic field on the transmission of TlBr and also of TlCl was investigated for circularly polarized light. No direct magnetoabsorption effect was observed in the first exciton peak in either case. Oscillatory magnetoabsorption was observed in both TlBr and TlCl starting at an energy slightly less than the sideband.

The superposition of the small oscillatory absorption on the rapidly varying sideband background poses some experimental problems. One would like as thick a film as feasible to enhance the oscillations, but this requires working over a wide optical-density range. In the present experiment, the films were thin enough that the whole sideband and part of the first peak could be displayed on one scale. This facilitated obtaining comparable curves of $I(H)$ and $I(0)$ (somewhat greater resolution might have been obtained with thicker films).

Figure 12 shows the observed magnetoabsorption for TlBr at several different field strengths. Similar results were found for TlCl. Some of the difficulties involved can also be seen in Fig. 12. As the field increases, the oscillations spread out and their amplitude increases. At low fields, one has a small bump lying on the steep sideband edge. Without the zero-field correction, the oscillatory peak is not fully discernable until it has pushed out into the flatter part of the sideband. Figure 13 presents the transmission change $I(H)-I(0)$ (in arbitrary units) on the left scale versus energy on the bottom. Peak position versus magnetic field is plotted in the same figure on the right scale. The normalized peak position in both cases was found to shift linearly with magnetic field in the resolvable range of 20–50 kG. The line slope is 5.8×10^{-5} eV/kG in TlBr and 2.9×10^{-5} eV/kG in TlCl.

The present magnetoabsorption data is not extensive enough to be entirely conclusive. Two interpretations are possible. The first attributes the oscillations in the continuum to Landau quantization perhaps with the singularities rounded by the electron-hole Coulomb interaction. If such were the case, the peaks would converge to the band gap and occur at the energies $E_g+(n+\frac{1}{2})\hbar\omega_c$, where E_g is the band gap, n the Landau quantum number, and ω_c the cyclotron frequency. The second possibility allows for a diamagnetic effect among the higher exciton states which at moderate fields appears linear in H. Exciton effects are therefore crucial as in the Elliott-Loudon theory.[15] This latter theory cannot be directly applied since the magnetic energy is comparable to, rather than very much greater

[14] R. Z. Bachrach, Ph.D. thesis, University of Illinois, 1969 (unpublished).

[15] R. J. Elliot and R. Loudon, J. Phys. Chem. Solid **15**, 196 (1960).

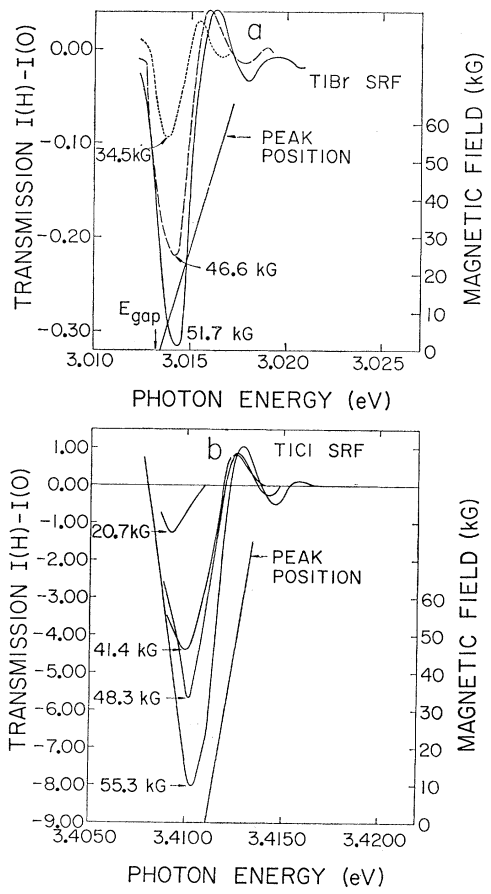

FIG. 13. The normalized magnetoabsorption spectra of TlBr and TlCl, and the first-peak position versus magnetic field.

than, the binding energy. Magnetoabsorption studies in these materials are a fertile area for additional work.[15a]

The extrapolation of the peak position lines in Fig. 13 to zero field yield binding energies which are in agreement with those determined from ϵ_2 and also from Faraday rotation. In the Faraday rotation result for TlBr, it was found that the $n=1$ and $n=2$ exciton line position did not change with field. Thus the zero-field intercept can approximately represent the series limit in either model. One would like to obtain a reduced exciton mass from the magnetoabsorption, but this cannot be done without a detailed theoretical analysis of what is a rather complex situation. Assuming that the peak spacing in TlBr is equal to the cyclotron energy, a reduced mass of $\mu^*=0.20$ is obtained. In TlCl the exciton reduced mass appears to be about twice as large $\mu^*\sim 0.4$.

The Faraday rotation was found to be linear in H and would therefore correspond to a linear Zeeman effect. The orbital contribution to the linear magnetic field effect for an exciton can be shown to be proportional to $(1/m_e^*-1/m_h^*)$.[16] The theory of Roth[17] for the effective g factor of excitons in semiconductors yields the following result for isotropic bands:

$$g_{\rm eff}=g_e-g_h=[2E_{\rm so}/(3E_{\rm gap}+2E_{\rm so})](1/m_e^*-1/m_h^*). \tag{27}$$

$E_{\rm so}$ is the spin-orbit splitting of the valence-band states. Equation (27) has been applied to results for CdSe.[18] From the point of view of spin-orbit interaction, our thallous halides have a similar band structure except that it is the conduction band which has large splitting rather than the valence band. If we apply Eq. (27) in the present case, an expression for the difference in reciprocal masses results:

$$\frac{1}{m_e^*}-\frac{1}{m_h^*}=\frac{g_{\rm eff}}{2E_{\rm so}/(3E_{\rm gap}+2E_{\rm so})}=g_{\rm eff}'. \tag{28}$$

From this last equation and the magnetoabsorption reduced mass

$$\frac{1}{\mu^*}=\frac{1}{m_e^*}+\frac{1}{m_h^*}, \tag{29}$$

the individual carrier masses can be estimated:

$$m_{e,h}^*=\frac{2}{1/\mu^*\pm g_{\rm eff}'}. \tag{30}$$

In the case of TlBr: $\mu^*=0.20$, $E_{\rm gap}=3.013$ eV, $E_{\rm so}=2.05$ eV, and $g_{\rm eff}'=2.2$, with the result that $m_e^*=0.28$ and $m_h^*=0.72$. A similar estimate was not made for TlCl because of the residual splitting in the first exciton peak and difficulties in interpreting the Faraday pattern.

Tamura and Masumi[19] have recently measured a cyclotron effective mass in TlBr of 0.53 free-electron masses. This does not agree very well with either electron or hole masses given above, but perhaps this is not very surprising. Our exciton reduced mass, as determined from magnetoabsorption data, is uncertain for reasons stated above, and Eq. (27) may not really be complete for our particular band situation. The spin contributions to $g_{\rm eff}$ may be quite different from what they are in CdSe,[18] and it is certainly true that the lattice (especially polaron effects) has not been taken into account in the theory of Roth.

Table III summarizes the known exciton parameters for TlBr and TlCl. Because of the above uncertainties,

[15a] Oscillatory magnetoabsorption has recently been reported in TlCl for higher fields than the present work. See S. Kurita and K. Kobayashi, J. Phys. Soc. Japan **26**, 1557 (1969).

[16] R. S. Knox, in *Solid State Physics*, edited by F. Seitz and D. Turnbull (Academic Press Inc., New York, 1963), Suppl. 5, p. 55.

[17] L. M. Roth, Phys. Rev. **118**, 1534 (1960); L. M. Roth, B. Lax, and S. Zwerdling, Phys. Rev. **114**, 90 (1959).

[18] R. G. Wheeler, and J. O. Dimmock, Phys. Rev. **125**, 1805 (1962).

[19] H. Tamura (private communication). See also H. Tamura and T. Masumi, Solid State Commun. **7**, 11 (1969).

TABLE III. Summary of exciton parameters. The optical results are assumed to yield the polaron masses given. The band masses were then estimated by means of polaron ϵ_{eff} and a_{eff}, and were computed from $\mathfrak{R}$ and μ^* assuming a hydrogenlike model (Eq. 32) theory.

	TlCl			TlBr		
Binding energy	11 ±2			6.5 ±1		
$\mathfrak{R}/\hbar\omega_{\text{LO}}$	0.50±0.1			0.46±0.06		
	Band	Polaron	Coupling constant	Band	Polaron	Coupling constant
Electron mass	0.32	0.53[a] 0.57[b]	2.4	0.18	(0.28)0.75[b]	2.1
Hole mass	1.01	2.72[a]	4.2	0.38	(0.72)	3.0
Reduced mass μ^*		0.44(0.4)			(0.20)	
Exciton mass M^*		3.25			(1.00)	
ϵ_s		37.6			35.1	
ϵ_0		5.1			5.4	
$\tilde{\epsilon}=\epsilon_s\epsilon_0/\epsilon_s-\epsilon_0$		5.9			6.4	
ϵ_{eff}		23.3			20.4	
a_{eff}		28 Å			54 Å	
Feynman electron		41.5 Å			77 Å	
Polaron radius[c] hole		16.3 Å			38 Å	
$\left(\frac{\hbar}{2m\omega_{\text{LO}}}\right)^{1/2}$ electron		23.0 Å			38.4 Å	
hole		14.0 Å			26.8 Å	

[a] Approximate values from cyclotron resonance; see J. Hodby, J. Borders, and F. C. Brown, Phys. Rev. Letters **19**, 952 (1967).
[b] From cyclotron resonance, H. Tamura and T. Masumi, Ref. 19.
[c] R. P. Feynman, Phys. Rev. **97**, 660 (1955).

the magnetoabsorption and g_{eff} results are listed in parentheses. In a previous paper,[1] arguments were presented that the sideband accompanying the first exciton peak was not, in fact, mainly due to higher exciton states. The magneto-optical experiments show this directly. The sideband in both TlBr and TlCl overlies the continuum and is separated from the $1s$ exciton state by approximately $\hbar\omega_{\text{LO}}$.

VI. EXCITONS MODEL FOR TlBr AND TlCl

One would like to be able to explain excitons in the thallous halides on the basis of the usual simple models. These, however, fail to accurately account for the observed binding energy and certain spectral details such as the phonon sideband. It is clear that corrections for the lattice must be made.

In a c.m. coordinate system, the Hamiltonian for a Wannier exciton[16] modified according to continuum polaron theory[20] is

$$H=\frac{P^2}{2M^*}+\frac{p^2}{2\mu^*}-\frac{e^2}{\epsilon_0 r}+\sum\hbar\omega_{\text{LO}}a_{\mathbf{k}}^{\dagger}a_{\mathbf{k}}$$
$$+\sum e^{i\mathbf{k}\cdot R}V_k(a_{\mathbf{k}}-a_{-\mathbf{k}}^{\dagger})(e^{i(m_h^*/M)\mathbf{k}\cdot\mathbf{r}}-e^{-i(m_e^*/M)\mathbf{k}\cdot\mathbf{r}}),$$

where

$$V_k=-\frac{i\hbar\omega_{\text{LO}}}{k}\left(\frac{\hbar}{2m_{e,h}^*}\right)^{1/4}\left(\frac{4\pi\alpha_{e,h}}{v}\right)^{1/2}, \qquad (31)$$

and where the coupling constant is given by

$$\alpha_{e,h}=\frac{e^2}{\hbar}\left(\frac{1}{\epsilon_0}-\frac{1}{\epsilon_s}\right)\left(\frac{m_{e,h}^*}{2\hbar\omega_{\text{LO}}}\right)^{1/2}.$$

[20] H. Frohlich, in *Polarons and Excitons*, edited by C. G. Kuper and G. D. Whitfield (Oliver and Boyd, Edinburgh, 1963).

The first two terms in Eq. (31) are the center of mass and relative kinetic energies, the third is the optically screened electron-hole Coulomb interaction, the fourth is the phonon field energy, and the last term is the exciton-LO-phonon interaction. The exciton-LO-phonon interaction vanishes if the electron and hole fixed lattice masses are equal. Although an exciton is electrically neutral, when the carrier masses are different, the moments of the spread-out charge distribution interact with the polarization field created by the LO phonons. Since the exciton energy levels have been referenced to zero energy, the crystal ground state is $-E$ band gap. In the absence of the exciton-LO-phonon interaction, the solutions of the above Hamiltonian are free excitons plus free phonons. The binding energy is analogous to that for a hydrogen atom except that a reduced mass μ^* and effective dielectric constant ϵ must be used:

$$\mathfrak{R}=13.6\mu^*/\epsilon^2\ \text{eV}, \qquad (32)$$

where $\mathfrak{R}$ is the rydberg. The situation is represented schematically in Fig. 14 which shows the energy of the zero- and one-phonon state plotted as a function $\mathfrak{R}/\hbar\omega_{\text{LO}}$, the exciton binding energy divided by the LO-phonon energy. No attempt has been made in the figure to indicate complicated renormalization changes or pinning effects near the continuum position. Two continua appear in the problem: One is the zero-phonon exciton continuum and the other is the free-phonon continuum which arises because of exciton dispersion. The $\mathfrak{R}/\hbar\omega_{\text{LO}}$ ratio appropriate to TlBr and TlCl is indicated in the figure.

The binding energies predicted by relation (32) are given in Table IV for different values of effective dielectric constant, or of screening ϵ and $\epsilon=\epsilon_0$ (reduced mass μ^*). Optical screening predicts much too deep an exciton. An alternative is to assume the lattice is fully

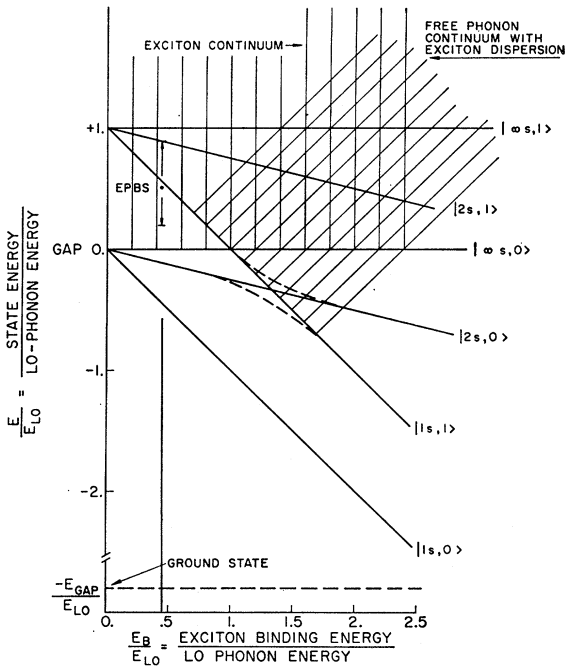

FIG. 14. A schematic representation of the exciton states as a function of binding energy showing the interaction of the zero- and one-phonon states.

able to screen the interaction and use the static dielectric constant ($\epsilon=\epsilon_s$) and polaron masses. Static screening of the Coulomb electron-hole interaction gives too small a binding energy, although it is better than optical screening. In large part, the lattice does follow the motion of electron and hole in the transition. It would appear that the appropriate eigenstates for optical excitations are those of the combined electron-lattice system. In a sense, the exciton seen in the thallous halides is a zero-phonon line with respect to LO phonons. Although the transition frequencies $\nu=E/h$ are high compared to the phonon frequencies ω_{LO} (7×10^{14} compared with 3×10^{12} cps), the frequency associated with the band gap is not the important one. The binding energy seen in optical absorption and the frequencies of internal motion of electron and hole are probably more significant. Also one should note that from the uncertainty principle and the observed exciton linewidth in TlBr (2 meV), the lifetime is at least as long as 2×10^{-12} sec, which is larger than phonon relaxation times. It may be that quite a bit of time is involved in transitions from the ground to exciton state after turning on the radiative perturbation.

TABLE IV. Exciton binding energy (meV).

	TlCl	TlBr	
Static ϵ_s	4.3	2.2	(μ^*=polaron mass)
Measured	11±2	6±1	
Haken	94	48	(μ^*=fixed lattice mass)
	152	75	(μ^*=polaron mass)
Optical ϵ_0	125	56	(μ^*=fixed lattice mass)
	230	93	(μ^*=polaron mass)

Another alternative is to use the Haken dielectric formulation of the exciton.[21] The Haken formula for effective dielectric constant provides an interpolation between optical and static screening within the framework of Eq. (31). The Haken potential is as follows:

$$V(r)=\frac{-e^2}{\epsilon(r)r}=-\frac{e^2}{\epsilon_0 r}+\frac{e^2}{r}\left(\frac{1}{\epsilon_0}-\frac{1}{\epsilon_s}\right)\times[1-\tfrac{1}{2}(e^{-r/\kappa_e}+e^{-r/\kappa_h})], \quad (33)$$

where

$$\kappa_{e,h}=\left(\frac{\hbar}{2m_{e,h}{}^*\omega_{LO}}\right)^{1/2},$$

and the masses are the fixed-lattice masses.

The Schrödinger equation cannot be solved analytically with the Haken potential. A Raleigh-Ritz variational calculation[22] was tried with a hydrogenic trial function. One seeks to minimize

$$E=\langle\Psi|H|\Psi\rangle \quad \text{with} \quad \Psi=(t^3/\pi)^{1/2}e^{-tr}. \quad (34)$$

The minimization condition is

$$2t-\frac{2}{\epsilon_0}-\frac{12t^2}{\bar{\epsilon}}\left(\frac{1}{(2t+1/\kappa_e)^2}+\frac{1}{(2t+1/\kappa_h)^2}\right)+\frac{16t^3}{\bar{\epsilon}}\left(\frac{1}{(2t+1/\kappa_e)^2}+\frac{1}{(2t+1/\kappa_n)^3}\right)=0. \quad (35)$$

Equation (35) was solved for the variational parameter t by computer. Although the result shown in Table IV is better than optical screening, the Haken screening formula gives much too deep a state. One of the reasons the Haken potential fails is that the $\kappa_{e,h}$ are quite large. The screening given by (33) within the measured Bohr radius is practically the full optical screening.

The above considerations make it clear that to understand the observed exciton binding energy, a more exact theoretical treatment is needed. The Rayleigh-Ritz procedure is really unsatisfactory because it gives no idea what the right variational wave function should be, or what the corrections to the potential are. The binding energy obtained from a variational calculation is very sensitive to the trial function near the origin. The free-exciton problem differs from the impurity problem in that the attractive potential is internal and must be calculated self-consistently. Several theories have been developed to calculate the ground-state energy of a bound polaron,[23] but the translationally

[21] H. Haken, Ref. 14, p. 295.
[22] A. Messiah, *Quantum Mechanics* (John Wiley & Sons, Inc., New York, 1961), p. 762.
[23] V. M. Buimistrov and S. I. Pekar, Zh. Eksperim. i Teor. Fiz. **32**, 1193 (1957); **33**, 1271 (1957) [English transls.: Soviet Phys.—JETP **5**, 970 (1957); **6**, 977 (1958)]; P. M. Platzman, Phys. Rev. **125**, 1961 (1962); T. D. Schultz, MIT Technical Report No. 9, 1956 (unpublished).

invariant form of these theories is difficult to apply.[24]

The remaining feature of the results to be discussed is the sideband observed accompanying the exciton. The experimental evidence leaves little doubt that the band is, in fact, a sideband and not higher exciton states. The sideband overlies the continuum and the ratio of the binding energy to the LO-phonon energy in both TlBr and TlCl is approximately 0.5. The shape of the sideband is little affected by changes in temperature and the $1s$-exciton sideband separation remains constant as the main peak shifts with temperature. In going from the bromide to the chloride, the binding energy scales with the reduced mass, and the peak sideband spacing scales with the LO-phonon energy. In both cases, the separation of the sideband from the main peak (ϵ_2 data) is reduced by about 5% from $\hbar\omega_{LO}$, although accurate values are difficult to determine because of the width and assymmetry of the peaks. The oscillator strength ratio of the main peak to the sideband is about 3:1 in TlBr and 4:1 in TlCl. Multiphonon peaks were not resolved, although there was some slight evidence of a very broad weak two-phonon band.

On the basis of a perturbative phonon-emission model for the sideband, one would expect a sideband edge starting at $\hbar\omega_{LO}$ and increasing proportional to the square root of energy (for a standard exciton E-versus-k dependence). One would therefore expect the phonon sideband to peak at an energy greater than $\hbar\omega_{LO}$ measured with respect to the first line. The free-phonon-emission model fails to accurately account for the observed sideband. The observed sideband starts well below $\hbar\omega_{LO}$ and peaks in the neighborhood of $\hbar\omega_{LO}$. It is conceivable that the LO frequency has to be renormalized or reduced in these problems. There are, however, other omissions of the theory so far.

The major deficiency of the perturbative picture is that it ignores the resonant interaction of the one-phonon state and the zero-phonon states. Recent calculations by Toyozawa and Hermanson[25] and by Larsen[26] have shown that the exciton-LO-phonon final-state interaction can completely alter the situation in the vicinity of the sideband. The treatment of Toyozawa and Hermanson is valid in the region $\mathcal{R}/\hbar\omega_{LO}\sim 0.9-1.5$. The effect is shown schematically in Fig. 14. The resonant exciton-LO-phonon interaction splits off a discrete state from the phonon continuum called the exciton-phonon bound state (EPBS). The split-off state, which has a mixed exciton and phonon character, has an energy lower than $\hbar\omega_{LO}$ and calculated oscillator strengths ranging up to 1:1 or 1:2 that of the zero-phonon $1s$-exciton line. As $\mathcal{R}/\hbar\omega_{LO}$ becomes smaller, the discrete exciton states regain their zero-phonon character. The problem of resonance between the zero-phonon continuum and the $|1s,1\rangle$ state remains, however, even to small ratios of $E_B/\hbar\omega_{LO}$. This case, which applies to the thallous halides, has recently been solved,[27] and the results appear to be in agreement with experiment.

VII. CONCLUSIONS

The previous experimental results on thin films of the thallous halides have been dominated by strain effects. The development of the SRF technique has permitted the probing of the intrinsic electronic structure in these materials. The initial interband transitions have been found to be direct and show strong exciton structure accompanied by a LO-phonon sideband. The sideband has been shown to overlie the continuum and not to be interpretable in terms of a simple LO-phonon emission model. The Faraday rotation has been measured and, although difficult to analyze, has provided an effective g value in TlBr. The Faraday rotation pattern further indicates that the hole has the heavier carrier mass in TlBr and TlCl and that the $J=1$ total angular momentum characterization of the first exciton transition is reasonable. Direct oscillatory magnetoabsorption has been observed for the first time in ionic-type materials and this opens the way for additional work.

ACKNOWLEDGMENTS

The authors would like to acknowledge many helpful discussions with Professor Y. Toyozawa, Dr. J. Hermanson, and Dr. A. B. Kunz. The comments and assistance of Dr. K. Kobayashi, Dr. E. J. Johnson, Dr. R. E. Hetrick, and D. Y. Le Corgne are also much appreciated.

[24] R. C. Brandt and F. C. Brown, Phys. Rev. **181**, 1241 (1969).

[25] Y. Toyozawa and J. C. Hermanson, Phys. Rev. Letters **21**, 1637 (1967).

[26] D. Larsen (unpublished). See also R. C. Brandt, D. M. Larsen, P. P. Crooker, and G. B. Wright, Phys. Rev. Letters **23**, 240 (1969).

[27] Y. Toyozawa, International Conference on Photoconductivity, Stanford, California, 1969 (unpublished).